Available online at www.sciencedirect.com
ScienceDirect
International Journal of Mass Spectrometry 261 (2007) 45–52
International Journal of Mass Spectrometry
www.elsevier.com/locate/ijms

Ion-mobility study of two functionalized pentacene structural isomers using a modified electrospray/triple quadrupole mass spectrometer

Svitlana V. Prada [a,b], Diethard K. Bohme [a,b], Vladimir I. Baranov [c,*]

[a] Department of Physics and Astronomy, Centre for Research in Mass Spectrometry, York University, Toronto, Canada M3J 1P3
[b] Department of Chemistry, Centre for Research in Mass Spectrometry, York University, Toronto, Canada M3J 1P3
[c] MDS SCIEX, 71 Four Valley Drive, Concord, Ont., Canada L4K 4V8

Received 13 June 2006; accepted 25 July 2006
Available online 7 September 2006

Abstract

We report ion-mobility measurements with a modified triple quadrupole mass spectrometer fitted with an ion molecule reactor (IMR) designed to investigate ion molecule reactivity in organic mass spectrometry. Functionalized pentacene ions, which are generally unreactive were chosen for study to decouple drift/diffusion effects from reactivity (including clustering). The IMR is equipped with a variable axial electrostatic drift field (ADF) and is able to trap ions. These capabilities were successfully employed in the measurement of ion mobilities in different modes of IMR operation. Theoretical modeling of the drift dynamics and the special localization of the large ion packet was successfully implemented. The contribution of the quadrupole RF field to the drift dynamics also was taken into consideration.

Keywords: Ion-mobility; Mass spectrometer; Ion molecule reactivity; Drift field

1. Introduction

A modified triple quadrupole mass spectrometer (MS) fitted with a simplified drift cell—linear ion trap (ion molecule reactor, IMR) is presented in this study. The IMR cell was designed primarily for the investigation of the analytical potential of ion molecule reactions in organic mass spectrometry [1–4]. In this work we focus on properties of the IMR as a drift cell. The IMR also can be used as a standard collision cell.

High precision drift cell set-ups are available primarily in research laboratories [5–7] where they are used to obtain fundamental ion mobility characteristics. In contrast, commercial and "near commercial" analytical tools such as field asymmetric waveform ion mobility spectrometers (FAIMS) [8–14] and ion mobility spectrometers (IMS) [15] in combination with MS and atmospheric pressure ionization (API) sources cannot provide ion mobility constants but are easy to use and praised as valuable analytical tools [16].

Similarly, to facilitate a wide spectrum of ion molecule reactions, the IMR cell is able to deliver a wide dynamic range of reaction gas number density, ion trapping time, RF and axial field conditions as well as multiple modes of operation and trapping. However, the instrument is not an IMS set-up; it is too "unsophisticated" to be a drift cell in its "academic" configuration and this simplicity implies that we cannot measure ion drift parameters, for example. Nevertheless, the IMR has a sufficiently good drift resolution capability and this adds to its analytical value and deserves special attention.

The class of organic compounds used in the drift experiments reported here was carefully chosen according to several considerations: (i) under normal API ion source conditions, the organic compound has to produce M^+ type ions exclusively (not protonated and not multiply charged); (ii) it should not form clusters in the interface region with a solvent or alkali metal ions; (iii) the M^+ ions should not be reactive toward residual water and methanol in the cell as well as toward a majority of other gases (such as oxygen, methane, nitric oxide and so on). These requirements are chosen to decouple the drift/diffusion effects from clustering, ion molecule-reactivity and selective trapping due to different RF stability conditions of product ions. Identifying compounds that would satisfy these requirements was chal-

* Corresponding author. Present address: IBBME, University of Toronto, 80 St. George Street, LM18, Ont., Canada M5S 3H6.
E-mail address: Vladimir.baranov@utoronto.ca (V.I. Baranov).

1387-3806/$ – see front matter © 2006 Elsevier B.V. All rights reserved.
doi:10.1016/j.ijms.2006.07.025

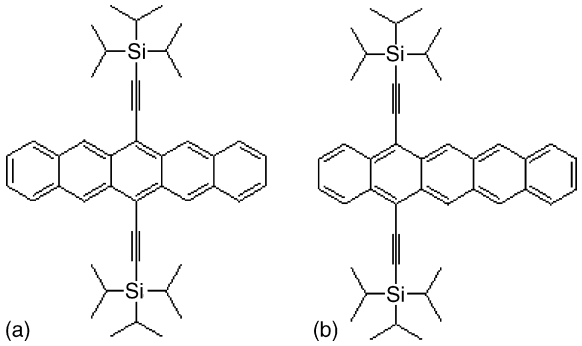

Fig. 1. Two types of functionalized pentacene derivatives: (a) symmetric 6,13-bis-[(triisopropylsilanyl)-ethynyl]-pentacene (TIPS) and (b) 5,14-bis-[(triisopropylsilanyl)-ethynyl]-pentacene (offset TIPS or o-TIPS).

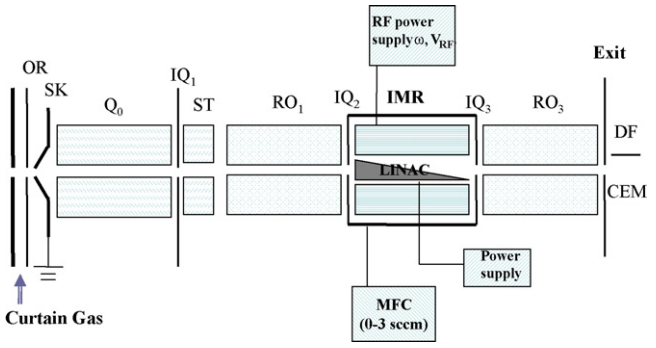

Fig. 2. Schematic representation of the IMR set-up: Q_0: RF-only ion guide; RO_1 and RO_3: dc offset of quadrupole mass analyzers; IQ_1, IQ_2 and IQ_3: electrostatic lenses; ST: short RF-only prefilter; IMR is encapsulated RF driven quadrupole; LINAC is linear accelerator-set of additional electrodes between the active quadrupole rods (0–0.4 V cm^{-1} range); RF power supply (0–250 V "peak-to-peak" range) and adjustable frequency (100 KHz to 5 MHz range); MFC is the mass flow controller up to 3 sccm (N_2); single-channel power supply.

lenging. We found that 6,13-bis-[(triisopropylsilanyl)-ethynyl]-pentacene (TIPS) largely satisfies the requirements. Additionally, TIPS has a structural isomer 5,14-bis-[(triisopropylsilanyl)-ethynyl]-pentacene (o-TIPS) with very close properties. Detection of the fine structural difference between TIPS and o-TIPS is a formidable challenge for any IMS set-up. These selected molecules (see Fig. 1) belong to a class of organic semiconductors that recently have been tested in molecular electronics devices such as organic thin film transistors (OTFT) [17–21].

2. Materials and methods

The selected organic compounds are functionalized pentacene derivatives (see Fig. 1). The TIPS compound and its isomer o-TIPS were synthesized at the Department of Chemistry, University of Kentucky, Synthetic Organic and Materials Chemistry Laboratory. They were prepared as described elsewhere [22]. The compounds were purified by repeated crystallization from acetone, then hexanes. In our sample preparation a mixture of toluene/methanol was used as a solvent. Stock solutions of TIPS and o-TIPS were made at concentrations equal to 940 nmol/ml in toluene/methanol 3:7 (v/v) mixtures. The solvents were degassed ultrasonically. Trifluoroacetic acid (TFA) 0.5% (v) and formic acid 0.5% (v) (separately) were added to the sample solutions and the solutions were examined for signal stability. After 48 h the ion signal derived from the formic acid solution drifted downwards by about 20%. In contrast, TFA containing solutions produced stable ion signals and these were used for further experiments. Toluene, methanol and TFA were purchase from Sigma–Adrich. Formic acid was purchase from AnalaR.

An electrospray ion source/triple quadruple mass spectrometer (based on API 3000, AB SCIEX) fitted with the IMR instead of a collision cell was employed in this study. The IMR cell is a pressurized RF driven quadrupole with a "Manitoba LINAC" (linear accelerator) [23], an independent RF power supply with means to control the waveform frequency and amplitude, and LabView based data acquisition and control software. The RF power supply is operated at user-selected RF amplitudes (0–250 V_{RF} "peak-to-peak", typically 200 V_{RF}) and frequencies (0.1–5 MHz, depending on desirable ion stability conditions). Such an arrangement allows sufficient flexibility in the selection of Mathieu stability conditions for a wide range of m/z values. To provide a uniform axial drift field (ADF), an additional four electrodes were inserted between the quadrupole rods [23], which provide the electrostatic field in the range 0–0.2 V cm^{-1} on the cell axis. The flow of the drift/reaction gas into the IMR cell is controlled up to 3 sccm (calibrated with N_2) by a mass flow controller (MFC Type 1179A, and Single-Channel Power Supply Type 246B, MKS Instruments, INC. Andover, MA, USA). The flow rates of the various collision/drift gases that were used in the IMR were determined by applying the effective gas correction factor (GCF) provided by the manufacturer. Additionally, the gas pressure inside of the IMR was cross-referenced with an independent drift experiment as described below. A schematic of the set-up is shown in Fig. 2.

3. Results and discussions

3.1. ADF/RF field impact on the ion energy and enthalpy of ion-molecule reactions

In the presence of the drift field, ions collide, drift and are trapped by the RF field concomitantly. The influence of the RF field ion stability conditions in the quadrupole field on the ion translational energy and outcome of ion-molecule reactions was discussed elsewhere [24,25] with different degree of simplification. Briefly, the frictional ion heating due to collisions increases the ion temperature T in comparison with the temperature of the buffer/reaction gas T_n:

$$3k_b(T - T_n) = m_n v_D^2 \quad (1)$$

Here k_b is the Boltzmann's constant, m_n the mass of the buffer/reaction gas molecule, v_D the drift speed. For example, the temperature difference is only 1 K for $v_D = 80$ m s^{-1}. Under "RF only" quadrupole field stability conditions after equilibra-

tion with buffer/reaction gas, an ion energy can be presented in the following form [24]:

$$E = \frac{ZeV}{4q}\left(\frac{r}{r_0}\right)^2 \nu_{21}^2(0,q) + k_b T \nu_{22}^2(0,q) + \frac{1}{2}k_b T \qquad (2)$$

Here q is a dimensionless quadrupole RF field stability parameter (in the first stability region changes in the range from 0 to 0.91), Ze the ion charge, V the amplitude of the RF drive, $2r_0$ the quadrupole electrode separation, r the location of the probing ion, $\nu_{21}^2(0,q)$ and $\nu_{22}^2(0,q)$ are dimensionless parameters which, for example, are equal to 0.2 and 1.18 for $q = 0.4$. For $q < 0.5$ the Eq. (2) estimates an ion energy below 0.5 eV close to the axis ($r \to 0$) of IMR. However, it grows exponentially with q and can be more than 10 eV. Although methodologies for the estimation of the RF field and the contribution of frictional ion heating to the ion energy are well developed, in this work we will explicitly employ experimental conditions that minimize these contributions, but this does not mean that these contributions cannot be used to promote normally endothermic ion-molecule reactions. However, a detailed consideration of this topic is outside the scope of this work.

3.2. Drift mode of the IMR operation

Every mode of the IMR operation starts with clearing the cell of trapped ions. A simple way to do this involves (i) the application of a strongly repulsive entrance lens IQ_2 potential to prevent an ion flow entering the cell; (ii) raising ADF to the maximum value and so forcing ions toward the exit lens ($U = 0.2\ \mathrm{V\ cm^{-1}}$ in our case); (iii) the application of a neutral or slightly attractive IQ_3 potential to guide the ion flow out the cell. It is feasible, and some times beneficial, to clear the IMR cell with the help of dipolar (or quadrupolar) resonance RF excitation, but we are not discussing this here.

The drift mode of the IMR operation allows ions to flow through the cell, does not include ion trapping, and is suitable for fast ion molecule reactions that take place at near the collision rate. The experimental arrangement of this mode of operation includes the following steps: (i) injection of ions into the cell for a short period of time with the entrance lens IQ_2 and the quadrupole rod offset RO_2 attractive (−15 V), ADF (0.05; 0.1; 0.2 V cm^{-1}) directed toward the exit lens, and a neutral or slightly attractive exit lens IQ_3 potential; (ii) raising the entrance lens potential to prevent the ion flow into the cell after a short period of time. The ion flow is "pulsed" through the cell. Parameters such as the ADF strength, the duration of the ion pulse, the gas flow (pressure), the type of drift/collision gas, etc. can be varied in this experiment.

A challenging experiment to differentiate between TIPS and o-TIPS isomers, which have identical m/z ratios but different geometries, was undertaken in this work. Ions were pulsed (duration 10 ms) into the IMR cell. The flow rate of the collision/drift gas was kept constant by MFC. Fig. 3(a) gives an example of the isomer separation by the difference in drift time in He gas. Fig. 3(b) provides a schematic representation of the drift mode of IMR operation.

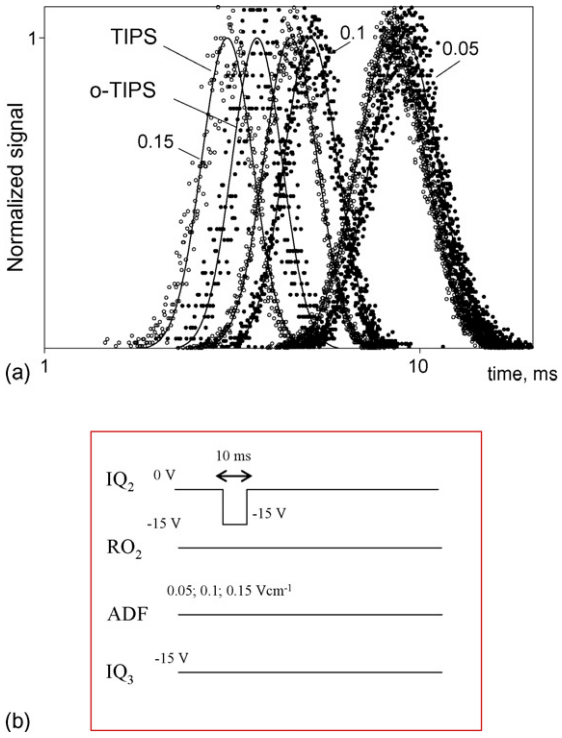

Fig. 3. (a) Separation of TIPS and o-TIPS is shown by differences in drift time in He at different axial drift field strength: 0.15, 0.10, and 0.05 V cm^{-1}. The best separation of the peaks can be seen at the highest drift field applied, 0.15 V cm^{-1}; $P_{He} = 9.7$ Torr; ion accumulation time is 1 ms; no trapping. (b) The schematic representation of the drift mode of IMR operation.

Mass spectra obtained in the continuous mode of low energy ion injection were carefully examined and did not reveal any evidence for the occurrence of ion-molecule chemistry in the drift cell. Therefore, we attribute all the observed effects to the drift of TIPS and o-TIPS ions.

3.3. Trapping mode of the IMR operation

In the second, trapping mode of the IMR operation, an ion packet is trapped in the middle of the cell for up to several seconds (1 s for the following experiments). This operational mode, which allows multiple collisions, is developed primarily for slow ion-molecule reactions and is expected to be important for large bio-organic ions. The diffusion equation for a rectangular ion packet (positioned in the centre of the cell with uniform number density n_0 and axial dimension equal to 2Δ) that moves with a drift speed v_D in a rarefied gas with a diffusion coefficient D and arrives on the detector at time t can be presented as following:

$$\frac{dn}{n_0} = \frac{v_D}{\sqrt{4\pi Dt}} e^{-((t-t_0)v_D)^2/4Dt}\, dt_0 \qquad (3)$$

Here t_0 is the time required for the ion packet to arrive at the detector with the drift speed v_D from a point in space without diffusion, L the half-length of the cell. Assuming that the ion packet is symmetrically localized in the IMR (see Fig. 4), Eq. (3) can be integrated over t_0 in an interval from $L - \Delta/v_D$ to

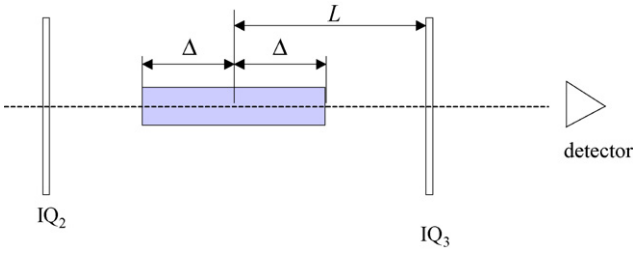

Fig. 4. The schematic representation of the ion packet. The assumption is made that the ion packet is symmetrically localized in IMR.

$L + \Delta/v_D$, resulting in the generalized error function:

$$\frac{n}{n_0} = \int_{\frac{L-\Delta}{v_D}}^{\frac{L+\Delta}{v_D}} \frac{v_D}{\sqrt{4\pi Dt}} e^{-v_D^2(t-t_0)^2/4Dt^2}\, dt_0$$
$$= \frac{1}{2}\left\{-\mathrm{erf}\left[\frac{L-\Delta-tv_D}{2\sqrt{Dt}}\right] + \mathrm{erf}\left[\frac{L+\Delta-tv_D}{2\sqrt{Dt}}\right]\right\}$$
$$= \frac{1}{2}\mathrm{erf}\left[\frac{L-\Delta-tv_D}{2\sqrt{Dt}}, \frac{L+\Delta-tv_D}{2\sqrt{Dt}}\right] \quad (4)$$

The experimental arrangement of this mode of operation includes the following stages: (i) injection of ions in the cell for a short period of time with the entrance lens and quadrupole rods offset attractive (−15 V), no ADF, and a strongly repulsive exit lens; (ii) raising of the entrance lens potential equal to the exit lens value; (iii) trapping for one second (typically); (iv) ejecting ions from the cell with the exit lens potential dropped to the quadrupole rods offset (or slightly attractive) and simultaneous application of ADF. Results for fitting experimental data with function (4) are presented in Fig. 5(a) for TIPS ions in He as a function of the arrival time on the detector. As one can see from (4), there are several parameters to be optimized: Δ - half-length of the ion packet, D and v_D. L was equal to 0.102 m. Despite the many simplifications in our model, Δ and D do not vary much as a function of ADF (as it should be) and were fixed at 0.0585 m and 0.418 $m^2\,s^{-1}$, respectively. The experimental results and fits are presented in Fig. 5(a).

The arrival time t_a on the detector can be determined from the solution of equation:

$$e^{(L-t_a v_D)\Delta/Dt} = \frac{L + t_a v_D + \Delta}{L + t_a v_D - \Delta} \quad (5)$$

and is used to differentiate the dead time t_c which was equal to the value obtained in the drift mode of the IMR operation. For TIPS ions under our experimental conditions t_a is presented in Fig. 5(b). A schematic representation of the trapping mode of the IMR operation is shown in Fig. 5(c).

The drift time that is obtained can be compared with the kinetic model (st) for ion mobility:

$$\mu_{st} = \frac{3Ze}{16}\sqrt{\frac{2\pi}{\mu k_B T_n}}\frac{1}{\sigma N_n}, \qquad t_{st} = \frac{L}{2\mu_{st}U} \quad (6)$$

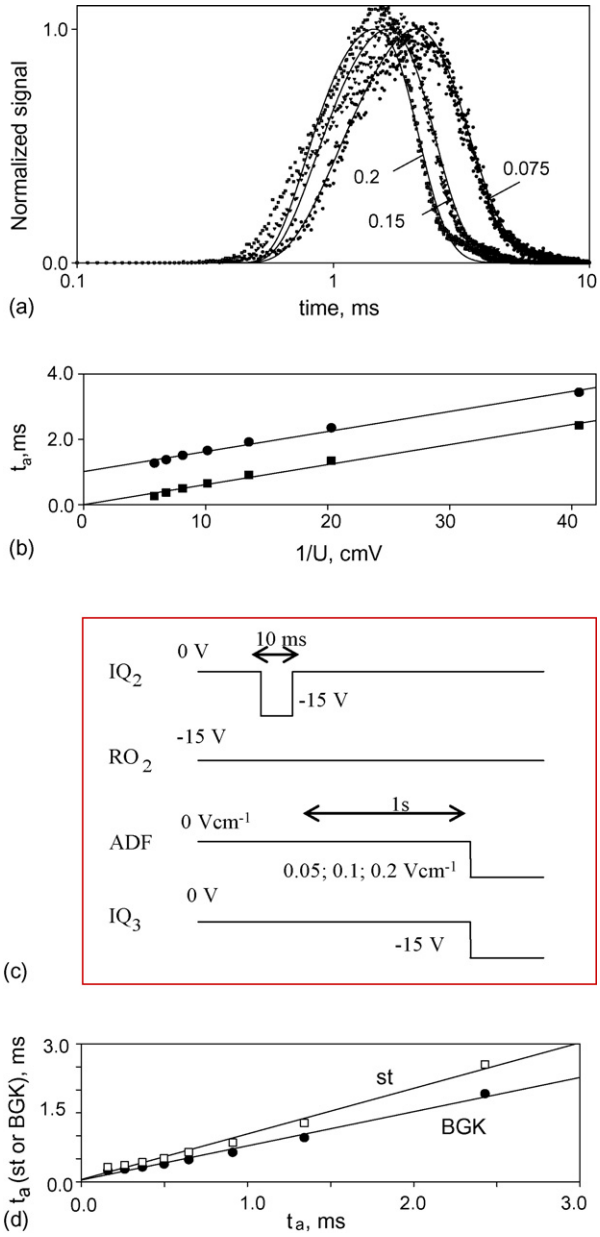

Fig. 5. (a) Results for fitting of experimental data with function (4) for TIPS ions in He as a function of the arrival time on the detector at different axial drift field strength: 0.2, 0.15 and 0.075 V cm^{-1}. P_{He} = 9.7 Torr; ion accumulation time is 1 ms; trapping time is 1 s. (b) The use of maximum arrival time on detector to determined the dead time. (c) Schematic representation of the trapping mode of the IMR operation. (d) Results of arrival time comparison with the kinetic model (st) for ion mobility μ and BGK model.

and the BGK model:

$$\mu_{BGK} = \frac{Ze}{4}\sqrt{\frac{2\pi}{\mu k_B T_n}}\frac{1}{\sigma N_n}, \qquad t_{BGK} = \frac{L}{2\mu_{BGK}U} \quad (7)$$

Here σ is the collision cross section, μ the reduced mass, N_n the gas number density, and T_n the temperature of the gas, and U is the ADF potential. To perform this comparison properly, the σ value should be measured independently. This was achieved using a well-characterized 20-segment quadrupole/ion mobility spectrometer cell with radial collisional focusing. The

20 quadrupole segments permit superimposition of ADF, typically linear, over the conventional quadrupole field in the radial direction [26]. The experimental conditions were measured to be $P = 0.505$ Torr in He, ADF (U) = 0.2 V cm^{-1}, the cell length $L = 20.2$ cm. The drift times for the two isomers were only slightly different ($t_{D\ (TIPS)} = 3.101$ ms, $t_{D\ (O\text{-}TIPS)} = 3.112$ ms) which translates into a small difference in the corresponding collisional cross sections (260 Å^2 for TIPS and 261 Å^2 for o-TIPS). Briefly, the collision cross sections were calculated using a well-known Mason–Schamp Eq. (6):

$$\sigma = \frac{3Ze}{16}\sqrt{\frac{2\pi}{\mu k_B T_n}}\frac{1}{\mu_{st} N_n}$$

Comparative results with our experiment are presented in Fig. 5(d) in favor of the kinetic model, perhaps not surprisingly, employing the Mason–Schamp equation.

It is experimentally challenging to measure pressure in the IMR. To be sure that our measurements are correct, the independent experiment was also used to derive a value of D for TIPS ions, which was equal to 0.418 m^2 s^{-1} for 9.7 mTorr of Helium. Under our experimental conditions, this value was used to confirm the calibration of the mass flow controller and the pressure gauge. Knowing the scaling factors of the mass flow controller and pressure gauge (provided by manufacturers), we were able to transform the flow rate values of different gases into the pressure values given in Table 1.

In a typical experiment of this kind with a selected gas, ions were pulsed (duration 10 ms) into the IMR cell. The flow rate of the collision/drift gas was kept constant by the MFC. Benzene, toluene, and water vapors over liquid substance were mixed with helium in a sample bag at ambient pressure; the vapor flow rates were estimated using the substance saturated vapor pressure under ambient temperature. The ion arrival time t_a on the detector was determined by fitting the experimental data with Eq. (4). Fig. 5(a) gives an example of fitted experimental drift results in helium for different ADF conditions. The arrival time of an ion packet traveling from IMR to the detector is a composite of the drift time t_D (the time that ions spent drifting in IMR) and the dead time (the time required to travel through other portions of the instrument). The list of gases used in the study and the resulting data are summarized in the Table 1.

Table 1
$U = 0.2$ V cm^{-1}

Compound	Gas	Pressure in IMR P (mTorr)	Drift time, t_d (ms)
TIPS	C_6H_6 (in He)	0.88	1.26
o-TIPS			1.27
TIPS	C_7H_8	0.35	1.35
o-TIPS			1.39
TIPS	O_2	6.63	1.19
o-TIPS			1.22
TIPS	N_2O	4.76	1.71
o-TIPS			1.77
TIPS	ND_3	4.89	1.39
o-TIPS			1.48
TIPS	He	9.70	1.41
o-TIPS			1.48
TIPS	H_2O (in He)	0.21	1.56
o-TIPS			1.62
TIPS	C_3H_6	2.76	1.26
o-TIPS			1.27
TIPS	CO	6.68	1.49
o-TIPS			1.57
TIPS	CO_2	4.68	1.55
o-TIPS			1.72
TIPS	H_2	6.76	1.65
o-TIPS			1.66
TIPS	NO (in He)	2.00	1.47
o-TIPS			1.53

The drift times of the two structural isomers were found to differ only marginally for most of the gases utilized in the IMR. However, some of the gases used in the study (NO, CO_2, CO, H_2O in He) demonstrated some separation.

As a result of its simplicity, the theoretical and experimental treatment has numerous limitations: first of all, it does not take the space charge into consideration—a very important practical concern was not to overfill the IMR cell during the injection stage. The space charge will manifest itself in a bimodal distribution of the ion signal as well as in a dependence of D on the injection time. Secondly, the suggested rectangular shape of the ion packet limits the accuracy of the fitting procedures. The negligible influence of the RF field under our experimental conditions already has been discussed but also has to be assessed in the case of complex ion-molecule reactions with product ions having simultaneously different stability conditions. Nevertheless, the model is sufficient to get some insight into the IMR operation in the trap mode.

3.4. Ion energy measurements following the trapping mode of the IMR operation

To explore the axial ion energy and its distribution after trapping/thermalization, a series of experiments were conducted under a wide range of experimental conditions with the exit aperture as a cutoff energy filter. As an example, the following results are presented for TIPS ions in helium (9.7 mTorr).

The experimental arrangements of this mode of operation after clearing of the IMR cell include the following stages: (i) injection of ions in the cell for a short period of time with the entrance lens IQ_2 and quadrupole rods offset RO_2 attractive, no ADF, and a strongly repulsive exit lens IQ_3; (ii) closing of the IMR cell by raising the entrance lens potential IQ_2, no ADF; (iii) trapping for one second; (iv) ejection of ions from the cell with RO_2 constant (−15 V), ADF and IQ_3 varied (as summarized in Table 2).

Prior to entering the high vacuum in the triple quadrupole section, ions are partially thermalized in Q_0-"RF only" quadrupole

Table 2

U (V cm^{-1})	IQ_3 (V)
0.025	−14.9 to −15.9
0.05	−14.0 to −15.0
0.1	−13.9 to −14.9
0.2	−13.5 to −14.5

under 7 mTorr of nitrogen introduced from the interface region. When ions enter the IMR cell, the Q_0 rods offset (normally −10 V) can be considered as a ground potential for ions. After trapping and thermalization, the IMR cell rods offset (normally −15 V) is a new ground potential for ions. For selected ADF potentials directed toward the cell exit, the exit lens potential can be used as a barrier that prevents some, or all, of the ions to leave the cell.

As was mentioned before, the translational ion energy has several contributors: thermal energy, frictional heating (caused by the ADF) and the RF field. The last one acts directly on the radial component of the ion motion, but due to multiple collisions with buffer gas, is equilibrated over all translational degrees of freedom.

The translational ion energy can be estimated using Eqs. (1) and (2). The parameters $\nu_{21}^2(0, q)$ and $\nu_{22}^2(0, q)$ are 0.01 and 1.01, respectively, when $a = 0$ and $q = 0.1$. For ions located 1 mm off the quadrupole axis, the RF field contribution leads to an effective temperature of the ions of 302 K. The ADF, obviously, contributes to the directional axial ion motion, but does not significantly affect ion temperature. For the maximum ADF value in He, the ion temperature can reach 316 K (for heavier collision/drift gas and low gas pressure, it could be higher). Under our intentionally selected experimental conditions, the frictional ion heating does not dramatically contribute to the total translational ion energy. Experimental data confirms this conclusion. As could be seen in Fig. 6(a), the energy distribution shifts towards larger drift values as the ADF increases, but does not change its width. The curves on the graph (stopping curves), are characteristic of the integral distribution of the axial ion energy: only ions with an axial energy above IQ_3 can be successfully detected. More accurately, the detector registers only ions that passed Q_3, but with the Q_3 rods offset potential fixed and strongly attractive, the effect can be neglected. The amount of translational energy ions gained due to the ADF can be calculated from the data as well and is demonstrated in Fig. 6(b). The axial drift energy linearly increases with increasing ADF, approximately up to 2 V. A schematic representation of the ion energy measurement experiment is shown in Fig. 6(c).

One could argue that such energy measurements are inherently insufficient since: the IQ_3 barrier is not strictly perpendicular to the ion flow; the detector is not positioned exactly next to IQ_3 (the effect of other electrostatic potentials leads to a noticeable decay in the ion signal before the cutoff potential is achieved); an ion packet is not under the same field conditions (in the vicinity of the entrance lens ions stay longer in the drift field). However, even under such limited experimental conditions, the contributions of different sources of ion energy can be controlled, estimated and measured.

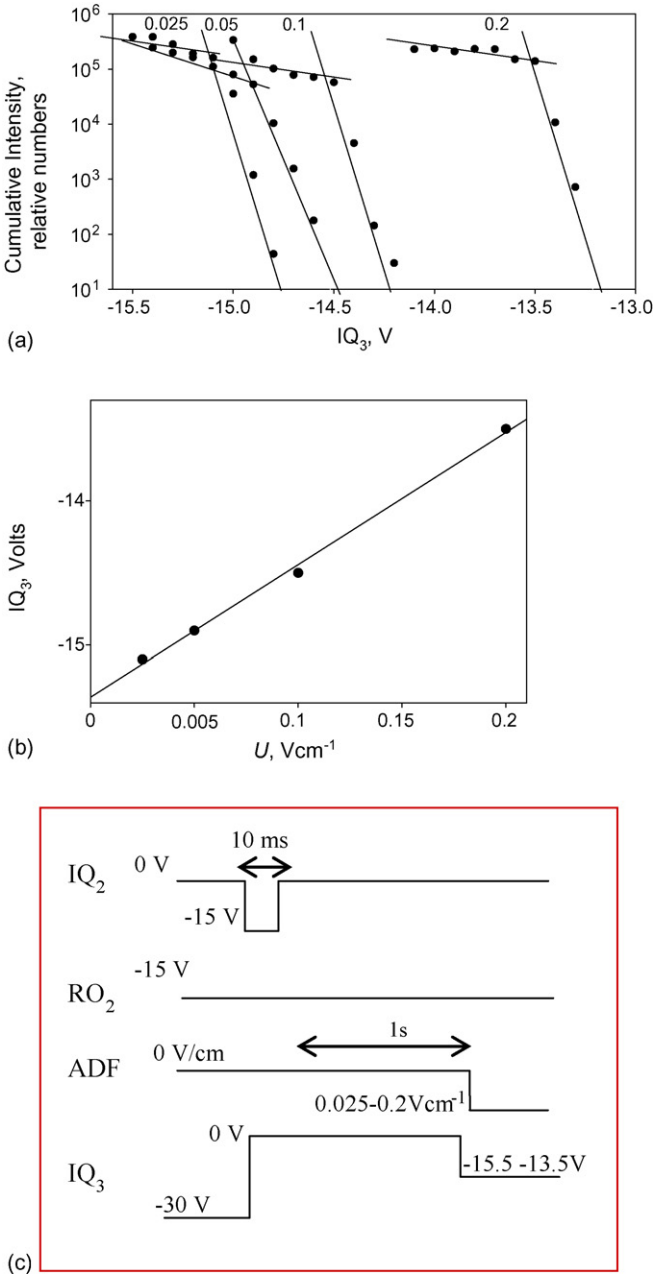

Fig. 6. (a) Ion energy distribution inside the IMR after thermalization for one second. The second part of the plot does not appear because the distribution itself is very narrow. (b) Potential energy barrier height vs. axial drift field strength. Drift of energy linearly increases with the increase in the ADF field. At 0 V cm^{-1} the exact value of IQ_3 is not −15 V but −15.3 V. This 0.3 V difference is an experimental deviation from the ions ground value. (c) Schematic representation of the ion energy measurement experiment.

3.5. Multiple axial pass mode of the IMR operation

What can one do when the drift effects or spatial stratification are not desirable but a slow rate of the ion molecule reaction requires long trapping times and the ADF must be used to evacuate ions from the IMR cell? A possible solution could be to use the trapping mode with a dynamic movement of the ion packet between the entrance and exit lenses. This mode of operation requires a periodic switching of the ADF polarity forcing the ion packet to drift back and forth. Momentary change of the drift field direction leads to the scramble of the separation achieved during the previous period. That could be done without a significant contribution to the enthalpy of an ion molecule reaction, as was demonstrated above. Therefore, the trapping and thermal effects of the ADF could be decoupled from the spatial separation. On the other hand, this mode of operation could be used to

heat complex organic ions frictionally throughout the trapping time, either separately or in combination with other forms of collisional heating such as dipolar excitation and shifting the RF stability conditions. Since this form of translational excitation could be controlled with high precision, it is particularly useful for preventing formation of clusters and other weakly bonded complexes.

This mode of the IMR operation includes the following stages: (i) injection of ions in the cell for short period of time with the entrance lens IQ_2 and quadrupole rods offset RO_2 attractive, the ADF directed toward the exit lens, and a strongly repulsive exit lens IQ_3; (ii) closing of the IMR cell by raising the entrance lens potential IQ_2; (iii) trapping for a desirable period of time with periodically changing the ADF direction; (iv) ejection of ions from the cell on the AFD cycle directed toward the exit lens with IQ_3 attractive.

The multiple pass mode of the IMR operation requires an experimental adjustment of the periodicity of the ADF switching. Empirically, the period depends on many parameters including gas pressure, the ADF strength (amplitude), RF stability conditions and mass of an ion. It is feasible to expect that geometric imperfections (asymmetry) of the IMR cell could lead to unequal times of the ion movement from IQ_2 to IQ_3 and back. Additionally, in order to avoid the signal decay due to defocusing of slow moving ions within the cell fringing fields, the amplitude of axial ion motion must be limited. Results under our experimental conditions are presented in Fig. 7(a). Fig. 7(b) provides a schematic representation of the IMR multiple pass mode of operation. It should be pointed out that there are many possibilities to arrange the multiple axial pass of ions in the IMR cell and this could be exploited for different purposes.

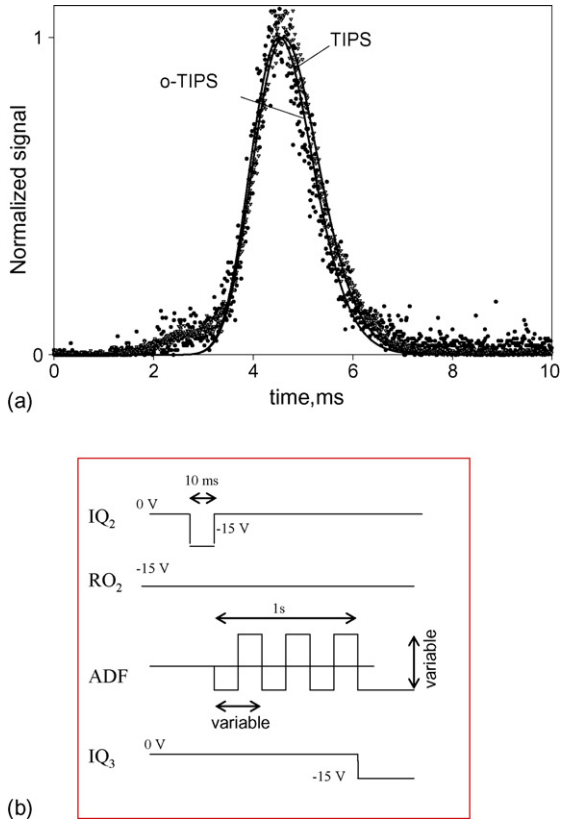

Fig. 7. (a) Comparison of TIPS and o-TIPS arrival times at the multiple pass mode of the IMR operation. (b) Schematic representation of the IMR multiple pass mode of operation.

4. Conclusions

Although the combination with a TOF mass spectrometer is more "natural" for transient signals typically observed in drift measurements, the simplicity and versatility of IMR in the proposed configuration offers a unique opportunity for combining the exquisite specificity of ion molecule reactions with the good resolution and adaptability of triple quadrupole mass spectrometry. It is very important to understand the fundamentals of the operation of the IMR cell, especially for distinguishing between changes in ion signal due to the drift/diffusion effects from those due to reactivity. The work reported here demonstrates that it is possible to do so with a high degree of confidence. One should expect that large organic ions with multiple degrees of freedom require somewhat longer reaction times due to a lower collisional/reaction efficiency in comparison, for example, with atomic ions. Therefore, special emphases should be given to longer trapping times and additional sources of enthalpy such as frictional heating due to the axial field and RF stability conditions. In this work, we have demonstrated several modes of operation of the IMR using non-reactive/non-clustering ions as a probe. This has provided useful general insight into ion trapping in the RF driven quadrupole cell. Additionally, a simple theoretical treatment is suggested to account for the properties of ion signal profiles after trapping in the IMR volume.

Acknowledgements

The authors would like to acknowledge MDS Sicex for the use of their equipment, with which all experiments were done, as well as the Canada Research Chair Program and the Natural Sciences and Engineering Research Council of Canada for financial support of the project. We also would like acknowledge Yuzhu Guo and Dr. K.W. Michael Siu, Centre for Research in Mass Spectrometry, York University, Toronto for their help in the determination of the collisional cross section of the isomers as well as Christopher R. Swartz and Dr. John E. Anthony, Department of Chemistry, University of Kentucky, Lexington for the synthesis of the TIPS and o-TIPS molecules.

References

[1] V.I. Baranov, S.D. Tanner, J. Anal. At. Spectrom. 14 (1999) 1133–1142.
[2] S.D. Tanner, V.I. Baranov, J. Am. Soc. Mass Spectro. 10 (1999) 1083–1094.
[3] S.D. Tanner, V.I. Baranov, U. Vollkopf, J. Anal. At. Spectrom. 15 (2000) 1261–1269.
[4] A. Dodonov, V. Kozlovsky, A. Loboda, V. Raznikov, I. Sulimenkov, A. Tolmachev, A. Kraft, H. Wollnik, Rapid Commun. Mass Spectrom. 11 (1997) 1649–1656.
[5] E.W. McDaniel, E.A. Mason, The Mobility and Diffusion of Ions in Gases, John Wiley & Sons, New York, 1973.

[6] P. Dugourd, R.R. Hudgins, D.E. Clemmer, M.F. Jarrold, Rev. Sci. Instrum. 68 (1997) 1122–1129.
[7] G.R. Asbury, H.H. Hill, J. Microcolumn Sep. 12 (2000) 172–178.
[8] I.A. Buryakov, E.V. Krylov, E.G. Nazarov, U.K. Rasulev, Int. J. Mass Spectrom. Ion Process. 128 (1993) 143–148.
[9] I.A. Buryakov, E.V. Krylov, A.L. Makas, E.G. Nazarov, V.V. Pervukhin, U.K. Rasulev, J. Anal. Chem. 48 (1993) 114–121.
[10] A.A. Shvartsburg, K.Q. Tang, R.D. Smith, J. Am. Soc. Mass Spectrom. 16 (2005) 1447–1455.
[11] R. Guevremont, G. Thekkadath, C.K. Hilton, J. Am. Soc. Mass Spectrom. 16 (2005) 948–956.
[12] A.A. Shvartsburg, K. Tang, R.D. Smith, J. Am. Soc. Mass Spectrom. 16 (2005) 2–12.
[13] D.A. Barnett, B. Ells, R. Guevremont, R.W. Purves, J. Am. Soc. Mass Spectrom. 13 (2002) 1282–1291.
[14] R. Guevremont, D.A. Barnett, R.W. Purves, J. Vandermey, Anal. Chem. 72 (2000) 4577–4584.
[15] Y.S. Sysoev, I.Y. Kartasheva, Meas. Tech. 46 (2003) 1036–1041.
[16] T. Wyttenbach, M.T. Bowers, Modern Mass Spectrom. 225 (2003) 207–232.
[17] J.E. Anthony, J.S. Brooks, D.L. Eaton, S.R. Parkin, J. Am. Chem. Soc. 123 (2001) 9482–9483.
[18] F.A. Hegmann, R.R. Tykwinski, K.P. Lui, J.E. Bullock, J.E. Anthony, Phys. Rev. Lett. 89 (2002) 2274031–2274034.
[19] O. Ostroverkhova, S. Shcherbyna, D.G. Cooke, R.F. Egerton, F.A. Hegmann, R.R. Tykwinski, S.R. Parkin, J.E. Anthony, J. Appl. Phys. 98 (2005) 1–12.
[20] O. Ostroverkhova, D.G. Cooke, S. Shcherbyna, R.F. Egerton, F.A. Hegmann, R.R. Tykwinski, J.E. Anthony, Phys. Rev. B: Conden. Matter Mater. Phys. 71 (2005) 1–6.
[21] S.V. Shcherbyna, D.K. Bohme, V.I. Baranov, A. Loboda, C.R. Swartz, J.E. Anthony, J. Am. Soc. Mass Spectrom. 17 (2006) 222–229.
[22] C.R. Swartz, S.R. Parkin, J.E. Bullock, J.E. Anthony, A.C. Mayer, G.G. Malliaras, Organic Lett. 7 (2005) 3163–3166.
[23] A. Loboda, A. Krutchinsky, O. Loboda, J. McNabb, V. Spicer, W. Ens, K. Standing, Eur. J. Mass Spectrom. 6 (2000) 531–536.
[24] V.I. Baranov, D.R. Bandura, S.D. Tanner, Int. J. Mass Spectrom. 247 (2005) 40–47.
[25] Y.Z. Guo, K.W.M. Siu, V.I. Baranov, J. Am. Soc. Mass Spectrom. 16 (2005) 957–966.
[26] Y.Z. Guo, J.X. Wang, G. Javahery, B.A. Thomson, K.W.M. Siu, Anal. Chem. 77 (2005) 266–275.